Egypt. J. Chem. **Vol. 65**, No. 12, pp. 409 - 419 (2022)

Egyptian Journal of Chemistry

http://ejchem.journals.ekb.eg/

Dual pharmacological targeting of *Mycobacterium tuberculosis* (Mtb) PKNA/PKNB: A novel approach for the selective treatment of TB illness

Ali N. Hussein[1], Mohammed FAWZI[2], Rasha Fadhel Obaid[3], Shiama Rabeea Banoon[4*], Emad Salaam Abood[5], Abdolmajid Ghasemian[6]

[1]*Department of Pharmacy, Osol Aldeen University College, Baghdad, Iraq*

[2]*AL-Manara College for Medical sciences, Department of Pharmacy, Maysan, Iraq*

[3]*Department of Biomedical Engineering, Al-Mustaqbal University College, Babylon, Iraq*

[4]*Department of Biology, College of Science, University of Misan, Misan, Iraq*

[5]*Medical physics Department, Hilla university college, Babylon, Iraq*

[6]*Noncommunicable diseases Research Centre, Fasa University of Medical Sciences, Fasa, Iran*

Abstract

As drug-resistant tuberculosis (TB) infections grow more widespread, antibiotics that inhibit *Mycobacterium tuberculosis* through a novel technique might be an important component of changing TB therapy. In *M. tuberculosis*, protein kinase A (PknA) and protein kinase B (PknB) are both essential serine-threonine kinases. These enzymes present an intriguing option for antimycobacterial drug discovery, given the large knowledge base in kinase inhibition. A recent experimental study shows that IMB-YH-8 acts as a dual PknA/ PknB inhibitor. However, its methods of selectivity and inhibition at the molecular level have yet to be fully elucidated. Molecular dynamics simulations have been used to probe the inhibitory mechanism and the selectivity impact, yielding important insights into the reported inhibitory effect. MD simulation reveled that IMB-YH-8 selectively targeted the hinge-binding pocket residues, with the acetophenone group interacting into the small hydrophobic pocket provided by Met143 and Val 23 in PknA, and by the analogue's residues Met 92 and Val 25 in PknB. Identification of the hinge-binding site residues could open the way toward the structure-based design of a novel structure-based design of highly PknA/PknB selective inhibition in the treatment of *Mycobacterium tuberculosis*.

Keywords: IMB-YH-8; UCSF Chimera; Molecular Molegro Viewer (MMV); MODELER 9.19; GPU amber 14 software; LEAP module.

1. Introduction

The global incidence of tuberculosis has reached an all-time peak, and the fast emergence of multidrug-resistant *Mycobacterium tuberculosis* strains has been identified as a key problem for global tuberculosis control efforts [1]. According to WHO 2018, an estimated 1.7 billion people are infected with *M. tuberculosis* during their lifetime [2]. In addition, there were 1.3 million deaths among who were HIV positive people [2,3].

Antibacterial chemicals that suppress bacteria via a unique mechanism may be beneficial in treating infections caused by drug-resistant strains.

In Mycobacterium TB, there are 11 serine/threonine protein kinases (Ser/Thr) (Mtb) [5,8]. Since both Protein Kinase A (PknA) and Protein Kinase B (PknB) play important roles in bacterial development in both culture media and Mtb infected host macrophages, they constitute appealing therapeutic targets [9–11].

PknA and PknB are known to have a significant impact on the mechanisms that determine cell shape and morphology, as well as cell division. Kang et al.[15] demonstrated that even minor differences in PknA or PknB levels have a negative effect on mycobacteria. PknA has been demonstrated to regulate morphological changes related with cell division, and overexpression results in elongated and branched structures [15,16]. PknB overexpression, on the other hand, has been linked to widening and

*Corresponding author e-mail: shimarb@uomisan.edu.iq

\Receive Date: 25 April 2022, Revise Date: 16 July 2022, Accept Date: 16 July 2022

DOI: 10.21608/EJCHEM.2022.135419.5981

bulging cells. Overexpression in both PknA, and PknB led to decline growth rate of the bacilli [15]. PknA and PknB consist of an ~ 270 an intercellular kinase domain. The kinase proteins are well studied for their druggable properties [39,40]. An ~60-70 amino acid juxta membrane domain, an ~20 amino acid transmembrane domain, and an ~20aa transmembrane domain connected to an extracellular domain. While the extracellular regions of PknA are relatively short (~70amino acid), the extra cytoplasmic domain of PknB contains iterative PASTA (penicillin binding protein and serine /threonine kinase associated)domains [5,17]. Dual targeting has the potential to significantly lower the frequency at which resistance develop [5,8].

In a recent study by Xu et al., the possibility of blocking Protein Kinase A (PknA) and Protein Kinase B (PknB) at their root was experimentally explored in an attempt to find an effective therapeutic strategy for T.B patients, regardless of bacterial growth for both Mtb infected host macrophage and culture medium [18].

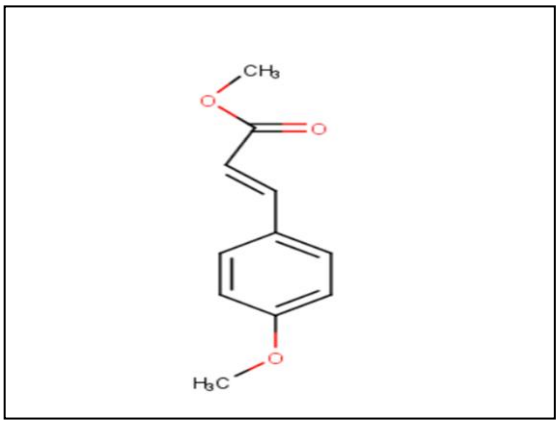

Figure 1: 2D structure of IMB-YH-8 [18]

Mycobacterium tuberculosis is a bacterium that causes tuberculosis [42].

IMB-YH-8 was shown to target protein kinase A (PknA) and protein kinase B (PknB) for therapeutic purposes [18]. Drug development has made extensive use of computer-aided drug design [41]. As a result, combinatorial techniques (in silico and in vitro) were used to identify the multi-target inhibitor IMB-YH-8, which was able to block the activities of both Protein Kinase A (PknA) and Protein Kinase B (PknB) simultaneously, Figure 2.

They predicted that this compound would have selective affinity to these two enzymes using molecular modelling and docking methods. To acquire a fundamental to the strategic design of innovative multi-target anti-tubercular medicines, further information on the inhibitory mechanisms of this molecule is needed, particularly at the hinge binding pockets of Protein Kinase A (PknA) and Protein Kinase B (PknB).

To this end, we use molecular dynamics (MD) simulation to investigate the processes and dynamics of interaction between IMB-YH-8, Protein Kinase A (PknA), and Protein Kinase B (PknB) in terms of selectivity, inhibition, and high binding affinity.

These findings, we hope, will aid the structure-based design of highly selective and innovative therapeutic drugs that can specifically and efficiently target tuberculosis Protein Kinase A (PknA) and protein kinase B (PknB)enzymes.

2. Computational methods

2.1. System preparation and MD simulations

RSCB Protein Data Bank [19–21] provided the X-ray crystal structures of *M. tuberculosis* PknA and PknB (PDB codes: 6P2Q and 2FUM, respectively). UCSF Chimera [22] and the Molecular Molegro Viewer (MMV) were used to build these structures for molecular dynamics (MD) simulation [23]. In order to lower the computational cost of this work, a monomer structure was chosen. MODELER 9.19 linked with chimaera software was then used to model the missing residues [24]. PubChem was used to find IMB-YH-8 [25].

The ligand was then given a hydrogen atom and the receptor was deleted. On the four prepared systems, all systems were then subjected to 100ns MD simulations as outlined in the Molecular dynamic simulation section.

2.2. Molecular Dynamic Simulations:

All of the molecular dynamic simulations were conducted using the GPU amber 14 software package [26]. Protein optimization and explicit solvation were performed using the built-in LEAP module, while the AMBER FF14SB force field was used to determine protein properties.

The systems were minimized for 2500 steps with a 100 kcal/mol enforced restraint, then 1000 steps of full minimization.

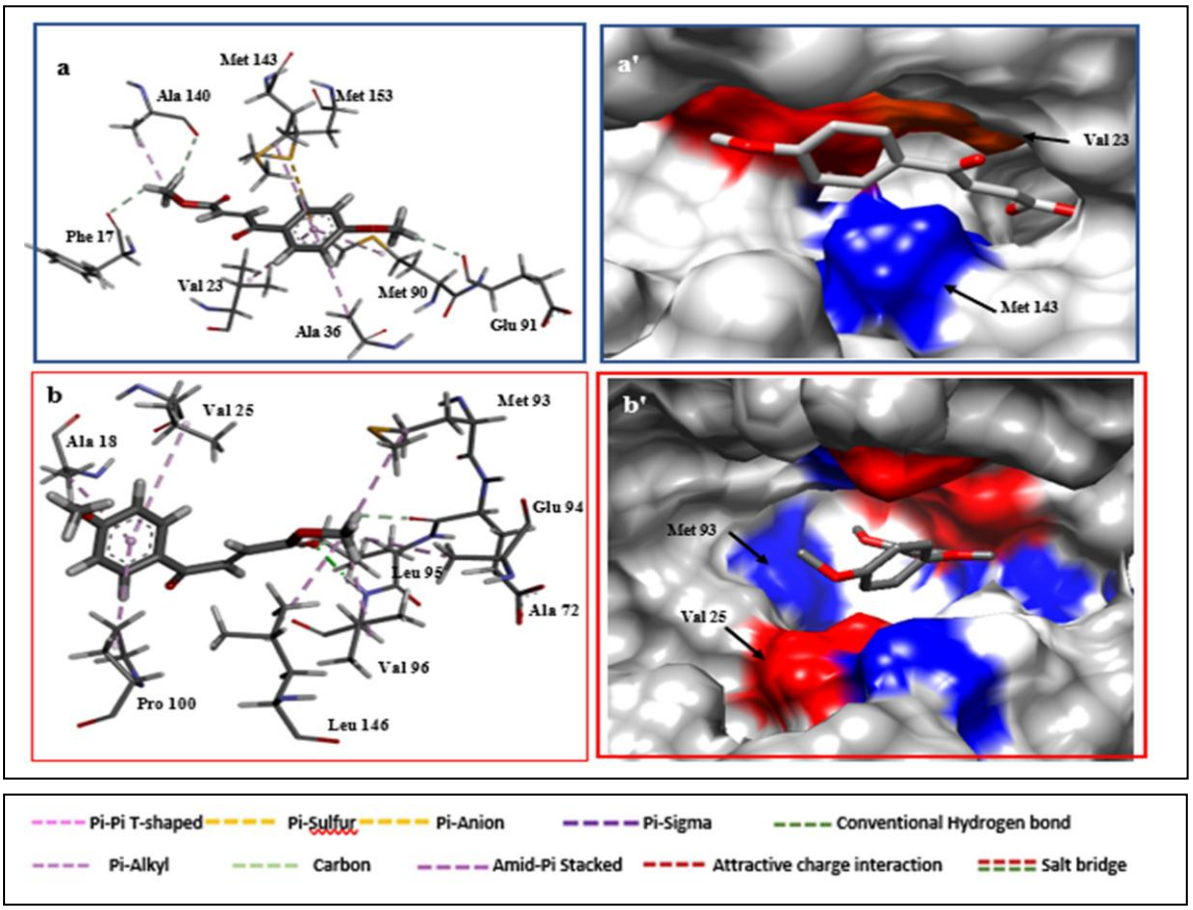

Figure 2: Molecular visualization of IMB-YH-8 at the hinge binding sites of [a] PknA [b] PknB. Inter-molecular interactions between IMB-YH-8 and hinge binding site residues in PknA and PknB are shown in a', and b' respectively. Black arrows show hydrophobic residues across the two proteins

The systems were then gradually heated for 50ps from 0K to 300K, with a potential harmonic restraint of 10 kcal/mol and a collision frequency of 1.0ps-1, to maintain a fixed number of atoms and fixed volume (NVT). Using the Berendsen barostat, the systems were then equilibrated without restraint at a temperature of 300K and a constant pressure of 1bar [27]. This was followed by 100ns of MD generation for each system, during which the SHACK method was employed to create hydrogen atom bonds.

2.3. Post-Dynamic Analysis

After saving the trajectories obtained by MD simulations every 1ps, they were analyzed using the AMBER 14 suit's CPPTRAJ [28] module. The Origin data analysis tool [29] and Chimera [22] were used to create all graphs and visualizations. These are based on a previous MD simulation procedure that was previously published [30].

Binding free energy calculations

Binding free energy calculations, which include both enthalpic and entropic contributions, are an essential end point method for elucidating the mechanism of binding between a ligand and a protein [31,32].

The free binding energy of the docked systems was computed using the Molecular Mechanics/GB Surface Area technique (MM/GBSA) to determine their binding affinity [33].

The binding free energy was calculated by averaging 1000 pictures from the 100 ns trajectory.

This approach estimated the free binding energy for each molecular species (complex, ligand, and receptor) can be expressed as:

$$\Delta G_{bind} = G_{complex} - G_{receptor} - G_{ligand} (1)$$

$$\Delta G_{bind} = E_{gas} + G_{sol} - TS \ldots\ldots\ldots\ldots (2)$$

$$E_{gas} = E_{int} + E_{vdw} + E_{ele} \ldots\ldots\ldots\ldots\ldots\ldots (3)$$

$$G_{sol} = G_{GB} + G_{SA} \ldots\ldots\ldots\ldots\ldots\ldots\ldots\ldots (4)$$

$$G_{SA} = \gamma SASA \ldots\ldots\ldots\ldots\ldots\ldots\ldots\ldots\ldots (5)$$

The terms Egas, Eint,Eele, and Evdw, respectively, stand for gas-phase energy, internal energy, coulomb energy, and van der Waals energy. The Egas was calculated using the FF14SB force field terms directly. The energy involvement of the polar states (GGB) and non-polar states (Gsol) was used to calculate the solvation free energy (Gsol) (G).

The solvent-accessible surface area (SASA) was used to determine the non-polar solvation energy (GSA), while the GB equation was used to get the polar solvation (GGB) contribution using a water probe radius of 1.4. The total entropy and temperature of the solute are denoted by the symbols S and T, respectively [37].

2.3.1. Per-Residue Free Energy Decomposition Analysis

Pre-residues breakdown was then used to assess the individual binding free energy contribution of residues in the ATP binding site to the stability and affinity of our compounds. As substantial residual energy contributions could indicate critical residues, this will provide greater insight into the basis of the inhibition observed by our compounds [38].

3. Results and Discussion

3.1. Molecular dynamic and system stability

To avoid disrupted motions and simulation artefacts, the system's unbound and bounded complex has to be stable during the 100ns MD production run. As a result, the root mean square deviations (RMSD) were tracked throughout the simulation to assess the systems' stability. After 30 ns (RMSD deviance 2.5 °A), both systems had reached convergence.

Figure 3A shows that the average RMSD values for the complete frames of the systems were 2.86, 2.69 for PknA-apo and PknA-IMB-YH-8, respectively, and 2.90,2.05 for PknB-Apo and PknB-IMB-YH-8. Figure 3B.

Furthermore, binding of IMB-YH-8 to these proteins resulted in a consistent pattern of structural change, involving an increase in deviation among the backbone atoms, as opposed to their unbound counterparts, which were structurally stable. PknA-apo, PknA- IMB-YH-8, PknB -apo, and PknB- IMB-YH-8 systems had average atomic fluctuations of 14.36, 10.41, 8.86, and 7.61, respectively. Figures 4A and B.

To observe the overall PknA and PknB proteins compactness upon ligand binding, the radius of gyration (ROG) was computed by measuring the mass-weighted root mean square distance of a collection of atoms from the centre of mass of complex during the MD simulation [34,35]. The difference in ROG values is observed at 70ns for the PknA system and 40ns for the PknB system, the average ROG values were 19.06Å, 18.80Å, 19.62Å and 19.50Å for PknA-apo, PknA- IMB-YH-8, PknB -Apo, and PknB- IMB-YH-8 systems respectively. The difference in ROG value is observed at 70ns for PknA system and 40ns for the PknB system, Figure 5 A, B.

Solvent-accessible surface area (SASA) of protein following ligand binding was calculated in order to get insight into the cooperation between the protein surface and solvent molecules and to receive insight into the connection of competence of the protein hydrophobic core. This was achieved by determining the solvent-accessible surface area of the protein, a property critical to its bimolecular stability [36]. The computed average SASA values were 13764.69Å, 13342.96Å, 13772.24Å and 13193.43Å for PknA-apo, PknA- IMB-YH-8, PknB -Apo, and PknB- IMB-YH-8 systems respectively Figure 5A and B. The SASA findings in conjunction with the RSMD observations, RMSF and ROG calculations further confirms that, PknA, and PknB exhibits more structural stability when it is bound to IMB-YH-8. Figure 6.

Presumably, disruption of the backbone atoms in PknA and PknB could highlight the mechanistic inhibitory activity of IMB-YH-8, since an induced loss of structural integrity in a protein correlate with loss of functionality.

3.2. Binding Free Energy Calculation-based Mechanism of Binding Interactions

To get insight into the binding energetics of IMB-YH-8 as dual PknA and PknB, the total binding free energy was determined. By taking snapshots from the trajectories of the compounds, the MM-GBSA software in AMBER14 was used to calculate the binding free energies.

As shown in Table 1, There was difference in the binding energy of IMB-YH-8 to PknB (-22.60kcal/mol) compared to that of PknA (-19.55kcal/mol), this indicated a more favorable binding of IMB-YH-8 toward the PknB compared with PknA. The computed binding energies correlated well with the experimental IC_{50} reported values [18].

The decomposition of the total free binding energy using the MM-GBSA method into individual contribution energy has provided more details in the understanding of the complex binding process. Van der Waals interaction energies are demonstrated to be pocket. We noticed that there are particular residues that interact consistently over 100ns.

This interaction should provide critical details and insight into the molecular basis for these two proteins' high binding affinity. Figure 8 shows the most striking and consistent interactions at the hydrophobic pocket into the hinge region, where the acetophenone ring of IMB-YH-8 interacted strongly with Met 143 for PknA and Met 93, Val 25 for PknB, explaining the selectivity and high binding affinity of IMB-YH-8 for PknB compared to PknA.

This could only imply that interaction with the Hinge-hydrophobic pocket is highly important for selectivity, the high binding affinity of IMB-YH-8and indicative of the basis and mode of dual inhibition.

4. Conclusion

The selectivity mechanism of IMB-YH-8 against PknA and PknB was investigated using comparative MD simulation and binding free energy responsible for positive binding free energies across all systems, while polar solvation energy terms contribute negatively to inhibitor binding.

3.3. Identification of the key residues responsible for inhibitor binding

The total binding energy of IMB-YH-8 toward protein kinase A (PknA) and protein kinase B (PknB) was further decomposed into the involvement of each site residues to acquire a better understanding of the critical residues engaged in the inhibition process. Figure 7 shows that residues Leu 15 (-1.30 kcal/mol), Val 23 (-1.63 kcal/mol), Met 143 (-1.12 kcal/mol), Met 153 (-1.192 kcal/mol) make the most favourable contribution to IMB-YH-8 to PknA binding, whereas residues Val 25 (-1.466 kcal/mol), Pro100 (-1.077 kcal/mol), Leu146 (-1.336 k336kcal/mol), Met 93(-0.571kcal/mol) for PknB.

3.4. Mechanism of binding interactions determined by the binding free energy calculation

To better understand how IMB-YH-8 interacts with PknA and PknB at the hinge-binding analysis in this study. The MM/GBSA method was used to determine the differential binding of IMB-YH-8 to these protein targets, revealing favourable interactions with G values of -19.55 kcal/mol (PknA) and -22.60 kcal/mole (PknB) (PknB). As previously reported, the similarity in binding free energies indicated parallel binding mechanisms and affinity. The Van der Waals energy component appears to be the dominant energy component driving this synergistic impact, according to the binding free energy component analysis. The total energies were decomposed into contributions from PknA and PknB active site residues, and it was discovered that Val25, Pro100, Leu146, and Met 93 are key residues in PknA, whereas Leu 15, Val23, Met 143, and Met 153 are significant residues in PknB.

Our findings are critical for understanding the molecular basis of the activity differential between IMB-YH-8 and PknA and PknB, as well as the development of a more effective selective inhibitor.

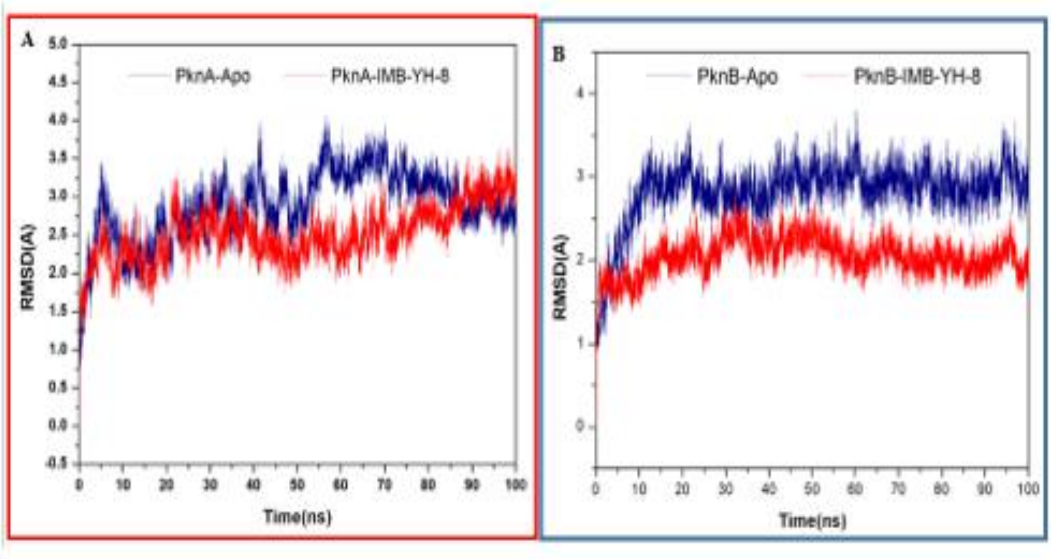

Figure **3**: Root-Mean-Square Deviation (RMSD) of Cα atoms of the protein backbone atoms showing the degree of stability upon IMB-YH-8 binding [A] PknA[B]PknB.

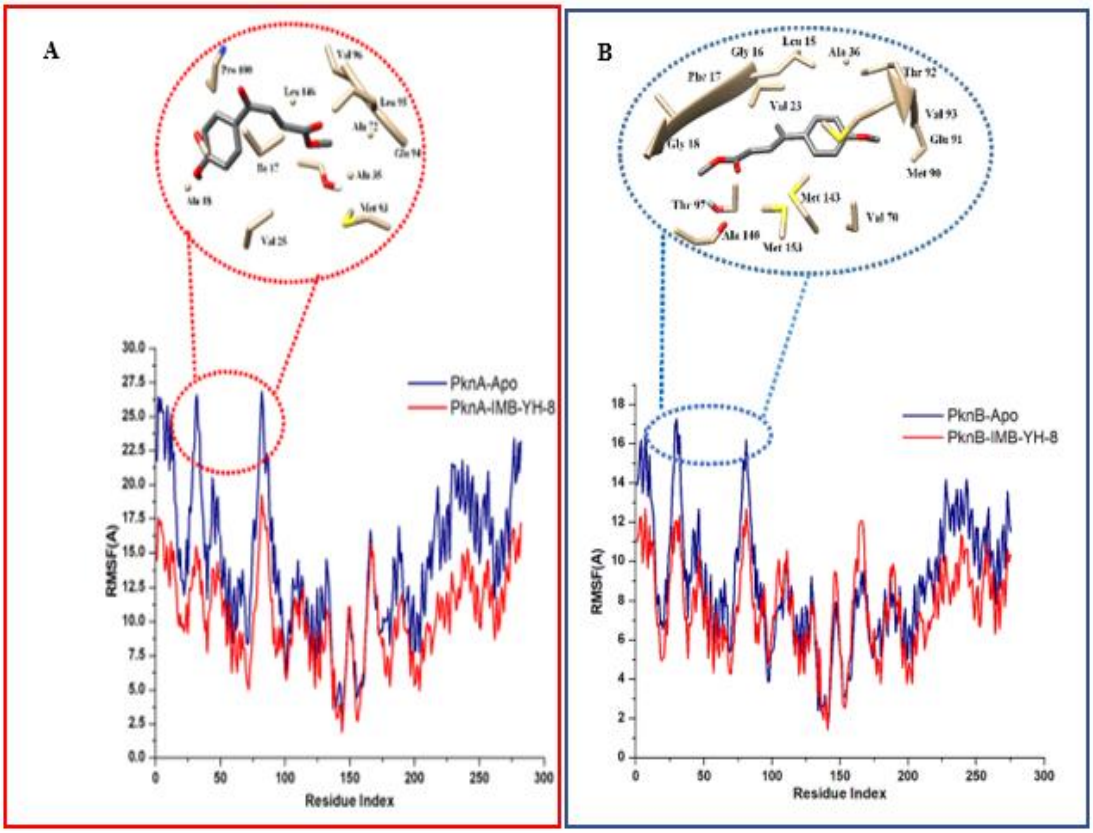

Figure 4: RMSF of each residue of the protein backbone Cα atoms shows the degree of flexibility upon IMB-YH-8 binding each of [A] PknA and [B]PknB.

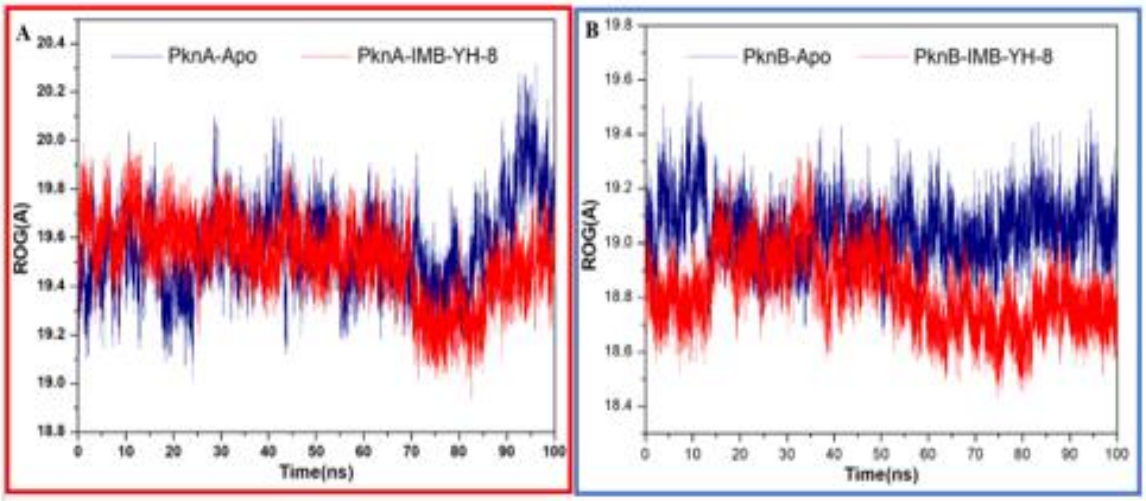

Figure 5: Radius of Gyration (ROG) of Cα atoms of protein residues shows the degree of compactness upon IMB-YH-8 binding [A] PknA[B]PknB.

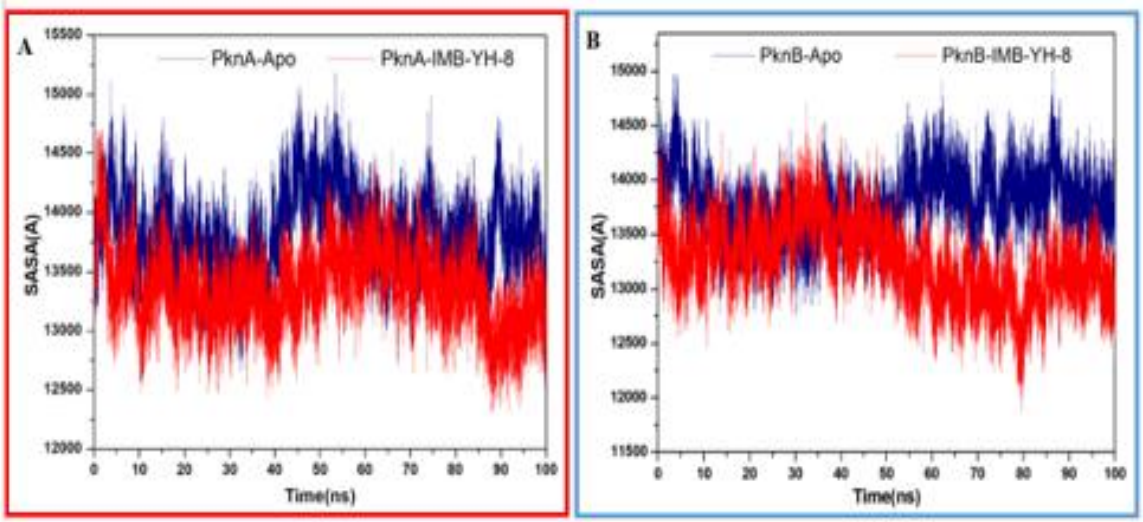

Figure 6: Solvent accessible surface area (SASA) of the backbone atoms relative to the starting minimized over 100ns for PknA-Apo, PknA-IMB-YH-8 systems.

Table 1Energy Components (kcal/mol)

Energy Components (kcal/mol)					
Complex	**Δ E_{vdW}**	**ΔE_{elec}**	**ΔG_{gas}**	**ΔG_{solv}**	**ΔG_{bind}**
PknA- IMB-YH-8	-27.35 ± 0.08	-5.40 ± 0.92	-32.76 ± 0.14	13.20 ± 0.09	-19.55 ± 0.08
PknB-IMB-YH-8	-31.05±0.07	-2.12±0.20	-33.17±0.23	10.57±0.18	-22.60±0.08

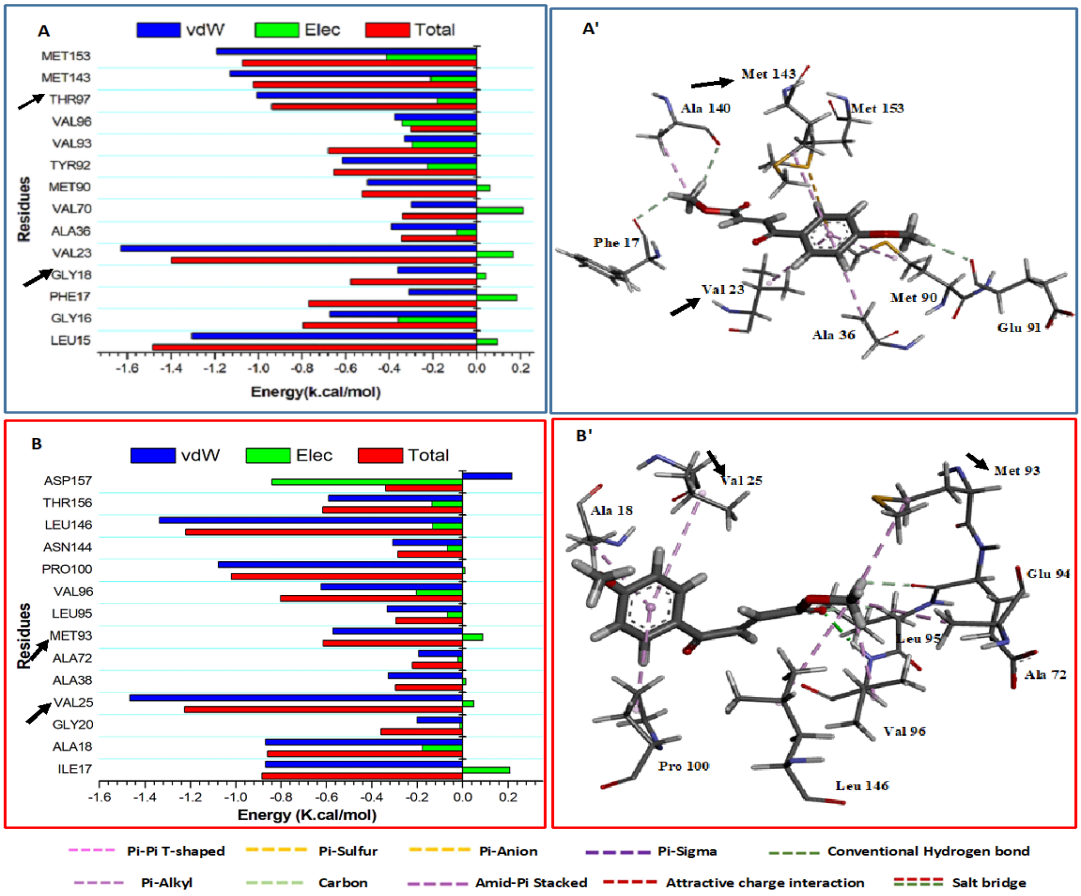

Figure 7: Per-residue decomposition plots showing the energy contributions to the binding and stabilization of IMB-YH-8 at the Hinge binding interaction of **[A]**PknA**[B]**PknB. Corresponding inter-molecular interactions are shown in **[A']**PknA, and**[B']** PknB while hinge binding interaction residues are indicated in black arrow.

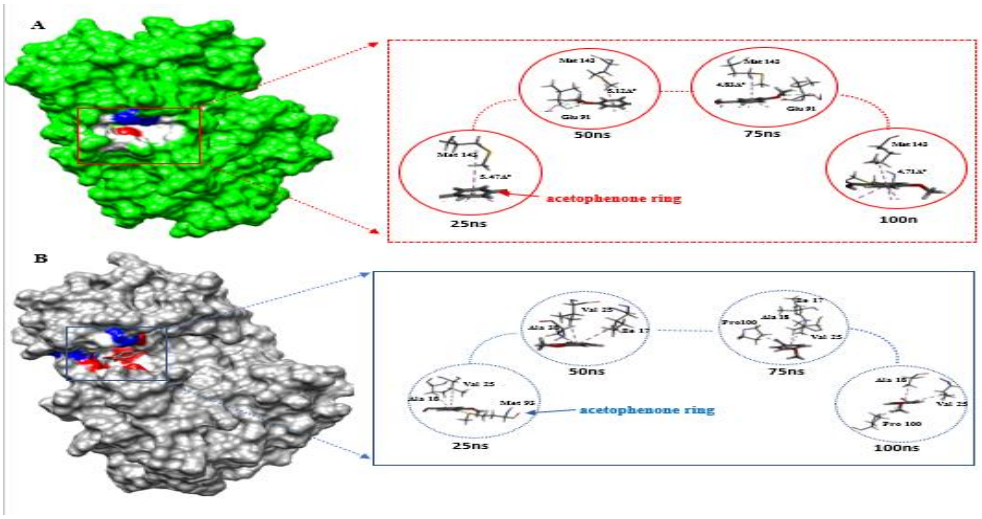

Figure 8: Systemic binding and interaction dynamics of IMB-YH-8 with hinge interaction binding residues in [A] PknA and [B] PknB showing steady interactions across the 100ns MD simulation time.

5. Conflicts of interest

"There are no conflicts to declare".

6. References

[1] Sandhu, Gursimrat K. "Tuberculosis: current situation, challenges and overview of its control programs in India." *Journal of global infectious diseases* 3, no. 2 (2011): 143.

[2] Talwar, Amish, Clarisse A. Tsang, Sandy F. Price, Robert H. Pratt, William L. Walker, Kristine M. Schmit, and Adam J. Langer. "Tuberculosis—United States, 2018." *Morbidity and Mortality Weekly Report* 68, no. 11 (2019): 257.

[3] Granich, Reuben, Somya Gupta, Bradley Hersh, Brian Williams, Julio Montaner, Benjamin Young, and José M. Zuniga. "Trends in AIDS deaths, new infections and ART coverage in the top 30 countries with the highest AIDS mortality burden; 1990–2013." *PloS one* 10, no. 7 (2015): e0131353.

[4] Cole, STea, R. Brosch, J. Parkhill, T. Garnier, C. Churcher, D. Harris, S. V. Gordon et al. "Deciphering the biology of Mycobacterium tuberculosis from the complete genome sequence." *Nature* 396, no. 6707 (1998): 190-190.

[5] Av-Gay Y, Everett M. The eukaryotic-like Ser/Thr protein kinases of Mycobacterium tuberculosis. Trends Microbiol [Internet]. Elsevier Current Trends; 2000 May 1 [cited 2018 Aug 27];8(5):238–44. Available from: https://www.sciencedirect.com/science/article/pii/S0966842X00017340

[6] Narayan A, Sachdeva P, Sharma K, Saini AK, Tyagi AK, Singh Y. Serine threonine protein kinases of mycobacterial genus: phylogeny to function. Physiol Genomics [Internet]. 2007 Mar 14 [cited 2018 Aug 27];29(1):66–75. Available from: http://www.physiology.org/doi/10.1152/physiolgenomics.00221.2006

[7] Molle V, Kremer L. Division and cell envelope regulation by Ser/Thr phosphorylation: Mycobacterium shows the way. Mol Microbiol [Internet]. 2010 Mar [cited 2018 Aug 27];75(5):1064–77. Available from: http://doi.wiley.com/10.1111/j.1365-2958.2009.07041.x

[8] Av-Gay Y, Jamil S, Drews SJ. Expression and characterization of the Mycobacterium tuberculosis serine/threonine protein kinase PknB. Infect Immun [Internet]. 1999 Nov [cited 2018 Aug 27];67(11):5676–82. Available from: http://www.ncbi.nlm.nih.gov/pubmed/10531215

[9] Sassetti CM, Boyd DH, Rubin EJ. Genes required for mycobacterial growth defined by high density mutagenesis. Mol Microbiol [Internet]. 2003 Apr [cited 2018 Aug 27];48(1):77–84. Available from: http://www.ncbi.nlm.nih.gov/pubmed/12657046

[10] Vieira, Tatiana F., Fábio G. Martins, Joel P. Moreira, Tiago Barbosa, and Sérgio F. Sousa. "In Silico Identification of Possible Inhibitors for Protein Kinase B (PknB) of Mycobacterium tuberculosis." *Molecules* 26, no. 20 (2021): 6162.

[11] Fernandez P, Saint-Joanis B, Barilone N, Jackson M, Gicquel B, Cole ST, et al. The Ser/Thr protein kinase PknB is essential for sustaining mycobacterial growth. J Bacteriol [Internet]. 2006 Nov 15 [cited 2018 Aug 27];188(22):7778–84. Available from: http://jb.asm.org/cgi/doi/10.1128/JB.00963-06

[12] Székely R, Wáczek F, Szabadkai I, Németh G, Hegymegi-Barakonyi B, Erős D, et al. A novel drug discovery concept for tuberculosis: Inhibition of bacterial and host cell signalling. Immunol Lett [Internet]. Elsevier; 2008 Mar 15 [cited 2018 Aug 28];116(2):225–31. Available from: https://www.sciencedirect.com/science/article/abs/pii/S0165247807003264

[13] Young TA, Delagoutte B, Endrizzi JA, Falick AM, Alber T. Structure of Mycobacterium tuberculosis PknB supports a universal activation mechanism for Ser/Thr protein kinases. Nat Struct Mol Biol [Internet]. Nature Publishing Group; 2003 Mar 27 [cited 2018 Aug 28];10(3):168–74. Available from: http://www.nature.com/articles/nsb897

[14] Ortiz-Lombardía M, Pompeo F, Boitel B, Alzari PM. Crystal structure of the catalytic domain of the PknB serine/threonine kinase from Mycobacterium tuberculosis. J Biol Chem [Internet]. American Society for Biochemistry and Molecular Biology; 2003 Apr 11 [cited 2018 Aug 28];278(15):13094–100. Available from: http://www.ncbi.nlm.nih.gov/pubmed/12551895

[15] Kang C-M, Abbott DW, Park ST, Dascher CC, Cantley LC, Husson RN. The Mycobacterium tuberculosis serine/threonine kinases PknA and PknB: substrate identification and regulation of cell shape. Genes Dev [Internet]. 2005 Jul 15 [cited 2018 Aug 28];19(14):1692–704. Available from: http://www.ncbi.nlm.nih.gov/pubmed/15985609

[16] Chaba R, Raje M, Chakraborti PK. Evidence that a eukaryotic-type serine/threonine protein kinase from *Mycobacterium tuberculosis* regulates morphological changes associated with cell

division. Eur J Biochem [Internet]. Wiley/Blackwell (10.1111); 2002 Feb 15 [cited 2018 Aug 28];269(4):1078–85. Available from: http://doi.wiley.com/10.1046/j.1432-1033.2002.02778.x

[17] Chakraborti PK, Matange N, Nandicoori VK, Singh Y, Tyagi JS, Visweswariah SS. Signalling mechanisms in Mycobacteria. Tuberculosis [Internet]. Churchill Livingstone; 2011 Sep 1 [cited 2018 Aug 28];91(5):432–40. Available from: https://www.sciencedirect.com/science/article/pii/S1472979211000680

[18] Xu J, Wang J-X, Zhou J-M, Xu C-L, Huang B, Xing Y, et al. A novel protein kinase inhibitor IMB-YH-8 with anti-tuberculosis activity. Sci Rep [Internet]. 2017 Jul 11 [cited 2018 Oct 25];7(1):5093. Available from: http://www.nature.com/articles/s41598-017-04108-7

[19] Ravala SK, Singh S, Yadav GS, Kumar S, Karthikeyan S, Chakraborti PK. Evidence that phosphorylation of threonine in the GT motif triggers activation of PknA, a eukaryotic-type serine/threonine kinase from Mycobacterium tuberculosis. FEBS J. Wiley/Blackwell (10.1111); 2015 Feb;282(8):1419–31.

[20] Wehenkel A, Fernandez P, Bellinzoni M, Catherinot V, Barilone N, Labesse G, et al. The structure of PknB in complex with mitoxantrone, an ATP-competitive inhibitor, suggests a mode of protein kinase regulation in mycobacteria. FEBS Lett. 2006;580(13):3018–22.

[21] Donini S, Ferraris DM, Miggiano R, Massarotti A, Rizzi M. Structural investigations on orotate phosphoribosyltransferase from Mycobacterium tuberculosis, a key enzyme of the de novo pyrimidine biosynthesis. Sci Rep. 2017;7(1):1180.

[22] Pettersen EF, Goddard TD, Huang CC, Couch GS, Greenblatt DM, Meng EC, et al. UCSF Chimera--a visualization system for exploratory research and analysis. J Comput Chem [Internet]. 2004 Oct [cited 2017 Jun 13];25(13):1605–12. Available from: http://doi.wiley.com/10.1002/jcc.20084

[23] Kusumaningrum S, Budianto E, Kosela S, Sumaryono W, Juniarti F. The molecular docking of 1,4-naphthoquinone derivatives as inhibitors of Polo-like kinase 1 using Molegro Virtual Docker. J Appl Pharm Sci. 2014;4(11):47–53.

[24] Webb B, Sali A. Comparative Protein Structure Modeling Using MODELLER. In: Current Protocols in Protein Science. Hoboken, NJ, USA: John Wiley & Sons, Inc.; 2016. p. 2.9.1-2.9.37.

[25] Kim S, Thiessen PA, Bolton EE, Chen J, Fu G, Gindulyte A, et al. PubChem substance and compound databases. Nucleic Acids Res. 2016;44(1):1202–13.

[26] Case DA, Cheatham TE, Darden T, Gohlke H, Luo R, Merz KM, et al. The Amber biomolecular simulation programs. J Comput Chem [Internet]. 2005 Dec [cited 2017 Aug 11];26(16):1668–88. Available from: http://www.ncbi.nlm.nih.gov/pubmed/16200636

[27] Berendsen HJC, Postma JPM, van Gunsteren WF, DiNola A, Haak JR. Molecular dynamics with coupling to an external bath. J Chem Phys [Internet]. American Institute of Physics; 1984 Oct 15 [cited 2017 Jun 21];81(8):3684–90. Available from: http://aip.scitation.org/doi/10.1063/1.448118

[28] Roe DR, Cheatham TE. PTRAJ and CPPTRAJ: Software for Processing and Analysis of Molecular Dynamics Trajectory Data. J Chem Theory Comput. American Chemical Society; 2013 Jul;9(7):3084–95.

[29] Seifert E. OriginPro 9.1: Scientific data analysis and graphing software - Software review. J Chem Inf Model. 2014;54(5):1552–1552.

[30] El Rashedy AA, Olotu FA, Soliman MES. Dual Drug Targeting of Mutant Bcr-Abl Induces Inactive Conformation: New Strategy for the Treatment of Chronic Myeloid Leukemia and Overcoming Monotherapy Resistance. Chem Biodivers [Internet]. 2018 Mar [cited 2018 Jul 17];15(3):e1700533. Available from: http://doi.wiley.com/10.1002/cbdv.201700533

[31] Raha K, Merz KMBT-AR in CC. Chapter 9 Calculating Binding Free Energy in Protein–Ligand Interaction. In Elsevier; 2005. p. 113–30.

[32] Ylilauri M, Pentikäinen OT. MMGBSA As a Tool To Understand the Binding Affinities of Filamin–Peptide Interactions. J Chem Inf Model. American Chemical Society; 2013 Oct;53(10):2626–33.

[33] Hou T, Wang J, Li Y, Wang W. Assessing the performance of the MM/PBSA and MM/GBSA methods. 1. The accuracy of binding free energy calculations based on molecular dynamics simulations. J Chem Inf Model. 2011;51(1):69–82.

[34] Pan L, Patterson JC, Deshpande A, Cole G, Frautschy S. Molecular Dynamics Study of Zn(Aβ) and Zn(Aβ)2. PLoS One [Internet]. Public Library of Science; 2013 Sep 27 [cited 2017 Jul 8];8(9):70681–8. Available from:

http://dx.plos.org/10.1371/journal.pone.0070681

[35] Wijffels G, Dalrymple B, Kongsuwan K, Dixon N. Conservation of Eubacterial Replicases. IUBMB Life [Internet]. Informa Healthcare; 2005 Jun 1 [cited 2017 Jul 8];57(6):413–9. Available from: http://doi.wiley.com/10.1080/15216540500138246

[36] Richmond TJ. Solvent accessible surface area and excluded volume in proteins. Analytical equations for overlapping spheres and implications for the hydrophobic effect. J Mol Biol [Internet]. 1984 Sep 5 [cited 2018 Apr 2];178(1):63–89. Available from: http://www.ncbi.nlm.nih.gov/pubmed/6548264

[37] Waheed, Sodiq O., Rajeev Ramanan, Shobhit S. Chaturvedi, Jon Ainsley, Martin Evison, Jennifer M. Ames, Christopher J. Schofield, Christo Z. Christov, and Tatyana G. Karabencheva-Christova. "Conformational flexibility influences structure–function relationships in nucleic acid N-methyl demethylases." *Organic & Biomolecular Chemistry* 17, no. 8 (2019): 2223-2231.

[38] Oluyemi, Wande M., Babatunde B. Samuel, Adeniyi T. Adewumi, Yemi A. Adekunle, Mahmoud ES Soliman, and Liselotte Krenn. "An Allosteric Inhibitory Potential of Triterpenes from Combretum racemosum on the Structural and Functional Dynamics of Plasmodium falciparum Lactate Dehydrogenase Binding Landscape." *Chemistry & biodiversity* (2022): e202100646.

[39] AL-OBAIDI, Zaid Mahdi Jaber, Awatef A. Ibrahim AL-ANI, and Dhurgham Qasim SHAHEED. "Synthesis, characterization, and biological evaluation of ibuprofen derivative against colon and breast cancer cell-lines." 2021, Patent.

[40] Al-Obaidi, Zaid Mahdi Jaber, Alaa A. Ali, and Tariq Hussien Mousa. "Synthesis of novel ibuprofen-tranexamic acid codrug: estimation of the clinical activity against HCT116 colorectal carcinoma cell line and the determination of toxicity profile against MDCK normal kidney cell line." *International Journal of Drug Delivery Technology* 9, no. 2 (2019).

[41] Al-Obaidi, Zaid Mahdi Jaber, Yasmeen Ali Hussein, Dunya AL-Duhaidahawi, and Hayder A. Al-Aubaidy. "Molecular docking studies and biological evaluation of luteolin on cerebral ischemic reperfusion injury." *Egyptian Journal of Chemistry* 65, no. 6 (2022): 1-2

[42] Koch, Anastasia, and Valerie Mizrahi. "Mycobacterium tuberculosis." *Trends in microbiology* 26, no. 6 (2018): 555-556.